Smart Structures and Systems, *Vol. 20, No. 3 (2017) 329-342*
DOI: https://doi.org/10.12989/sss.2017.20.3.329

Influence of electro-magneto-thermal environment on the wave propagation analysis of sandwich nano-beam based on nonlocal strain gradient theory and shear deformation theories

Ali Ghorbanpour Arani*, Mahmoud Pourjamshidian[a] and Mohammad Arefi[b]

Department of Solid Mechanics, Faculty of Mechanical Engineering, University of Kashan, 87317-53153, Kashan, Iran

(Received January 26, 2017, Revised July 30, 2017, Accepted August 3, 2017)

Abstract. In this paper, the dispersion characteristics of elastic waves propagation in sandwich nano-beams with functionally graded (FG) face-sheets reinforced with carbon nanotubes (CNTs) is investigated based on various high order shear deformation beam theories (HOSDBTs) as well as nonlocal strain gradient theory (NSGT). In order to align CNTs as symmetric and asymmetric in top and bottom face-sheets with respect to neutral geometric axis of the sandwich nano-beam, various patterns are employed in this analysis. The sandwich nano-beam resting on Pasternak foundation is subjected to thermal, magnetic and electrical fields. In order to involve small scale parameter in governing equations, the NSGT is employed for this analysis. The governing equations of motion are derived using Hamilton's principle based on various HSDBTs. Then the governing equations are solved using analytical method. A detailed parametric study is conducted to study the effects of length scale parameter, different HSDBTs, the nonlocal parameter, various aligning of CNTs in thickness direction of face-sheets, different volume fraction of CNTs, foundation stiffness, applied voltage, magnetic intensity field and temperature change on the wave propagation characteristics of sandwich nano-beam. Also cut-off frequency and phase velocity are investigated in detail. According to results obtained, UU and VA patterns have the same cut-off frequency value but AV pattern has the lower value with respect to them.

Keywords: higher order shear deformation; Reinforcement CNT composite; sandwich nano-beam; wave propagation; nonlocal strain gradient theory

1. Introduction

The considerable advantages offered by carbon nano-tube reinforced composites (CNTRCs) rather than other composite materials have prompted an increased use of sandwich structures with CNTRC face-sheets in nano and micro fields (Ghorbanpour Arani *et al.* 2015). Composite materials are basically manufactured from two phases: reinforcing phase and matrix phase. Since introduction of CNTRC, Some investigations on various aspects of the different structures made of these materials have been performed (Eltahera *et al.* 2016, Ghorbanpour Arani *et al.* 2014, Ghorbanpour Arani *et al.* 2016, Ghorbanpour Arani *et al.* 2016, Rabani Bidgoli *et al.* 2015).

Li *et al.* (2015) developed an analytic model of small-scaled functionally graded (FG) beams for the flexural wave propagation analysis based on the nonlocal strain gradient theory. The size-dependent wave propagation analysis of double-piezoelectric nano-beam-systems (DPNBSs) based on Euler–Bernoulli beam model was carried out by Ghorbanpour Arani *et al.* (2014). They concluded that the imposed external voltage is an effective controlling parameter for wave propagation of the coupled system. Ma *et al.* (2017) investigated the dispersion behavior of waves in magneto-electro-elastic (MEE) nano-beams based on Euler model and Timoshenko nano-beam model and calculated the cut-off frequency that was function of various loads. In the other research, a sandwich beam with periodic multiple dissipative resonators in the sandwich core material was investigated for broadband wave mitigation and/or absorption by Chen *et al.* (2017). Mitra *et al.* (2016) presented an analytical–numerical method, based on wavelet spectral finite elements (WSFE), in order to study the nonlinear interaction of flexural waves with a breathing crack present in a slender beam. The propagation and attenuation properties of waves in ordered and disordered periodic composite Timoshenko beams were studied by Wu *et al.* (2016). They considered the effects of axial static load and structural damping in aforementioned investigation.

Also, they assumed that beam is resting on elastic foundations and subjected to moving loads of constant amplitude with a constant velocity.

In other hand, Timoshenko beam theory or first order shear deformation beam theory (FSDBT) and various high order shear deformation beam theories (HOSDBTs) such as Reddy beam or parabolic shear deformation beam theory (PSDBT), trigonometric shear deformation beam theory (TSDBT), exponential shear deformation beam theory (ESDBT), hyperbolic shear deformation beam theory (HSDBT), and Aydogdu shear deformation beam theory

*Corresponding author, Professor
E-mail: aghorban@kashanu.ac.ir
[a]Ph.D. Student
[b]Assistant Professor

ISSN: 1738-1584 (Print), 1738-1991 (Online)

(ASDBT) were presented by investigators to analyze the beams (Ansari *et al.* 2014, Arvin and Bakhtiari-Nejad 2013, Li *et al.* 2014, Reddy 2007, Simsek and Reddy 2013a, Y. Yang and Lim 2012). To improve mechanical and physical behaviors of structures, it is proper to use the composite materials. carbon nanotube reinforcement composites (CNTRCs) can be used to reinforce the polymer composites (Esawi and Farag 2007). Developing of these material properties makes that the CNTRCs achieve various applications in micro and nano systems (Ashrafi and Hubert 2006). Recently, many researchers focused on the problems that concern with FG-CNTRC. For example, some researchers investigated on different interesting subjects such as thermal stresses analysis; linear and nonlinear vibration and dynamic responses of different structures in thermal environments (Ghorbanpour Arani *et al.* 2015, Ghorbanpour Arani *et al*. 2012). Rafiee *et al.* (2014) carried out an investigation on nonlinear stability and resonance response of the imperfect plate made of piezoelectric FG-CNTRC subjected to various combined electrical and thermal loads. Mohammadimehr *et al.* (2015) investigated the effects of different patterns and aligning of CNTs in height direction of the visco-elastic double-bonded polymeric nano-composite plate on dimensionless natural frequency. They found that the volume fractional CNTs in nano-composite can be used as a main control parameter to set the natural frequency of micro/nano electromechanical systems. Topic such as wave propagation is of important issues in analysis of micro/nano electromechanical systems.

Recently, the influences of the small scale parameters were considered by several researchers in nano and micro structures. In aforementioned studies in order to incorporate the small scales in equations of motions, various theories such as the strain gradient theories and Eringen's differential nonlocal model were used (Lim *et al.* 2015). Classical continuum models (Shakeri *et al*. 2006, Zhang and Paulino 2007), nonlocal continuum theory (Ebrahimy and Hosseini 2016, Shafiei *et al.* 2016), strain gradient theory (Gholami *et al*. 2014, Rahmani and Jandaghian 2015), and modified couple stress models (Ansari *et al.* 2014, Nateghi and Salamat-talab 2013) were used by researchers for analysis of nano/micro systems. In addition, regarding to the strain gradient theory, the strain energy is a function of the strain and curvature tensors (Yang *et al.* 2002). As can be seen, these mentioned theories express the basic various assumptions in order to explain the small-scaled systems.

Lim *et al*. (2015) carried out an investigation and showed the nonlocal and strain gradient parameters basically described two different physical properties of the structures in nano and micro scales. They have presented a new approach and theory to develop the strain gradient and nonlocal theories named the nonlocal strain gradient theory (NSGT). Actually, this theory is a combination of the two aforementioned theories that incorporated both small scales parameters namely nonlocal and strain gradient parameters. Based on the NSGT, Liew *et al.* (2008) analyzed the wave propagation in a SWCNT by molecular dynamics simulations.

In present study, the influences of electro-magneto-thermal environments and various shear deformation theories are investigated on wave propagation characteristics in sandwich nano-beam with CNTRC face-sheets using nonlocal strain gradient theory. It is assumed that beam rests on a Winkler-Pasternak foundation. Also, to align CNTs as symmetric and asymmetric in top and bottom face-sheets with respect to natural geometric axis of the sandwich nano-beam, various patterns are employed in this analysis. Hamilton's principle is used to derive governing equations of motion. The small scales parameters are included in equations of motion by using the NSGT.

Afterwards, the analytical method is applied to extract solution for phase velocity in terms of important parameters of the problem. Our results show the influence of important parameters such as length scale parameter, nonlocal parameter, various patterns and volume fraction of the CNTs in face-sheets, parameters of Pasternak's foundation, applied voltage, magnetic intensity field and temperature increment on the phase velocity and cut-off frequency of sandwich nano-beam. Furthermore, the effect of various shear deformation theories is discussed on the characteristics of wave propagation in detail.

2. Properties of material

In this section, the materials properties of sandwich nano-beam are expressed in detail. The schematic of the nano-beam and aligning CNTs in its face-sheets in symmetric and asymmetric forms is presented in Fig. 1. The core and face-sheets of beam are made from piezoelectric materials and CNTRC in which matrix is piezoelectric. To calculate the effective properties of CNTRC, the Mori–Tanaka scheme or the rule of mixtures can be used (Natarajan *et al.* 2014). In this investigation to compute the effective material properties of face-sheets, the rule of mixtures with correction factors is employed. The properties of the CNTRC (Young's modulus (E^{rc}), expansion coefficient (α^{rc}), visco-elastic coefficient (τ_d^{rc}) and density (ρ^{rc}) of the reinforced composite) are expressed by (Rafiee *et al*. 2014)

$$\begin{aligned} E^{rc} &= \eta_1 V_{cn} E_{11}^{CN} + V_m E^m \\ G^{rc} &= \eta_1 V_{cn} G^{CN} + V_m G^m \\ \alpha^{rc} &= V_{cn} \alpha_{11}^{CN} + V_m \alpha^m \\ \tau_d^{rc} &= V_{cn} \tau_d^{CN} + V_m \tau_d^m \\ \rho^{rc} &= V_{cn} \rho^{CN} + V_m \rho^m \end{aligned} \tag{1}$$

In above relations, η_1, E_{11}^{CN}, G^{CN}, α_{11}^{CN}, τ_d^{CN} and ρ_{11}^{CN} are the CNTs efficiency parameter, the Young's modulus, the shear modulus, the expansion coefficient, the visco-elastic coefficient and density of the CNTs, respectively and E^m, G^m, α^m, τ_d^m and ρ^m are the corresponding properties for the matrix.

It is noted that superscripts rc and m denote the reinforcement composite (used in face-sheets) and matrix, respectively. In addition, V_{CN} and V_m characterize volume fractions of the CNTs and matrix. V_{CN} and V_m are related by $V_{CN} + V_m = 1$ (Shen and Zhang 2012). The distribution of the CNTs along the face-sheets are given by

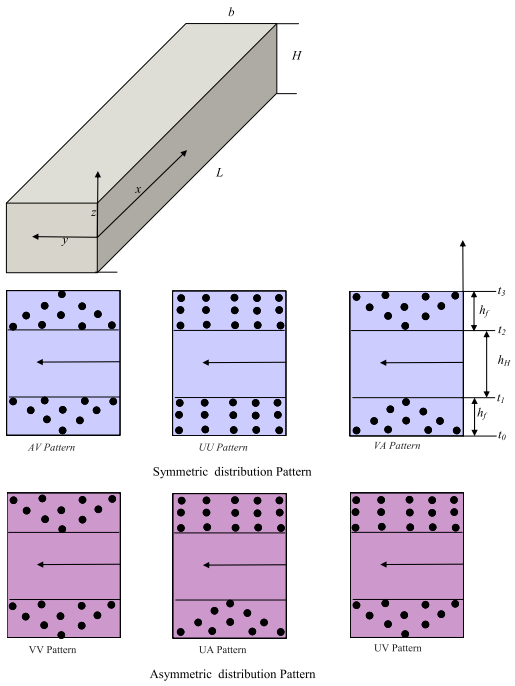

Fig. 1 Sandwich nano-beam with CNTRC face-sheets and attached coordinate system

$$V_{CN}^{t}=2\frac{(t_2-\bar{z})}{(t_2-t_3)}V_{CN}^{*}$$
$$V_{CN}^{b}=2\frac{(t_1+\bar{z})}{(t_1-t_0)}V_{CN}^{*},\quad\Rightarrow\quad for\ \ FG(VA)\ \ pattern$$

$$V_{CN}^{t}=2V_{CN}^{*}$$
$$V_{CN}^{b}=2V_{CN}^{*},\qquad\Rightarrow\quad for\ \ UD\ \ pattern \tag{2}$$

$$V_{CN}^{t}=2\frac{(t_3-\bar{z})}{(t_3-t_2)}V_{CN}^{*}$$
$$V_{CN}^{b}=2\frac{(t_0+\bar{z})}{(t_0-t_1)}V_{CN}^{*},\quad\Rightarrow\quad for\ \ FG(AV)\ \ pattern$$

In which V_{CN}^{t} and V_{CN}^{b} represent the volume fractions of the CNTs in top and bottom face-sheets, respectively. t_0 and t_3 are $\bar{z}$ coordinate of top and bottom face of the beam and also t_1 and t_2 are $\bar{z}$ coordinate of interface between top/bottom face-sheets and core of the beam, respectively. Furthermore, V_{CN}^{*} can be calculated as

$$V_{CN}^{*}=\frac{w_{CN}}{w_{CN}+\left(\frac{\rho^{CN}}{\rho^{m}}\right)-\left(\frac{\rho^{CN}}{\rho^{m}}\right)w_{CN}} \tag{3}$$

In which, w_{CN} is the mass fraction of the CNTs.

3. Formulation

The displacement field based on higher order shear deformation beam theory (HSDBT) is expressed as:

$$\bar{u}(\bar{x},\bar{z},\bar{t})=u_0(\bar{x},\bar{t})-\bar{z}\frac{\partial w_0(\bar{x},\bar{t})}{\partial\bar{x}}+\varphi(\bar{z})\gamma(\bar{x},\bar{t})$$
$$\bar{w}(\bar{x},\bar{z},\bar{t})=w_0(\bar{x},\bar{t}) \tag{4}$$

In which, $\bar{u}$ and $\bar{w}$ are axial and transverse displacement components, u_0 and w_0 are axial and transverse displacement of mid-surface. In addition $\varphi(\bar{z})$ is a function of $\bar{z}$ that presents the transverse shear and stress distribution along the thickness of the beam (Simsek and Reddy 2013b). Selection of $\varphi(\bar{z})$ is performed based on various beam theories as follows (Li *et al*. 2014)

$\boldsymbol{\varphi(\bar{z})}$	**Theory**
0	Euler- Bernoulli theory
$\bar{z}$	FSDBT or Timoshenko
$\bar{z}\left(1-\frac{4\bar{z}^2}{3H^2}\right)$	PSDBT
$\frac{h}{\pi}\sin\left(\frac{\pi\bar{z}}{H}\right)$	TSDBT
$H\sin\left(\frac{\bar{z}}{H}\right)-\bar{z}\cosh\left(\frac{1}{2}\right)$	HSDBT
$\bar{z}\exp\left(-2\left(\frac{\bar{z}}{H}\right)^2\right)$	ESDBT
$\bar{z}\alpha^{\frac{-2\left(\frac{\bar{z}}{H}\right)^2}{\ln\alpha}}$ *in which* $\alpha=3$	ASDBT

(5)

Also in Eq. (4) $\gamma(\bar{x},\bar{t})$ is the transverse shear strain of any point on the neutral axis (Simsek and Reddy 2013a) and is specified as

$$\gamma(\bar{x},\bar{t})=\frac{\partial w_0(\bar{x},\bar{t})}{\partial\bar{x}}-\phi(\bar{x},\bar{t}) \tag{6}$$

In above equation, $\phi(\bar{x},\bar{t})$ is the total bending rotation of the cross sections at any point on the neutral axis. The strain-displacement relation considering the thermal strain is expressed as

$$\varepsilon_{\bar{x}\bar{x}}=\frac{\partial u_0}{\partial\bar{x}}-\bar{z}\frac{\partial^2 w_0}{\partial\bar{x}^2}+\varphi\left(\frac{\partial^2 w_0}{\partial\bar{x}^2}-\frac{\partial\phi}{\partial\bar{x}}\right)-\alpha(\bar{z})\Delta T$$
$$\varepsilon_{\bar{x}\bar{z}}=\frac{\partial\varphi}{\partial\bar{z}}\left(\frac{\partial w_0}{\partial\bar{x}}-\phi\right) \tag{7}$$

In which, ΔT is the temperature increase that is equal to $\Delta T = T - T_0$. Where, T_0 is the initial temperature. In the present study, it is assumed that the electric potential is the sum of cosine function and a linear function. Then the electric potential can be written as (Arefi and Zenkour 2016, Arefi and Zenkour 2016)

$$\tilde{\Phi}\left(\bar{x},\bar{z},\bar{t}\right)=\cos\left(\beta\bar{z}\right)\bar{\Phi}\left(\bar{x},\bar{t}\right)+\frac{2\bar{z}V_0}{h_H} \tag{8}$$

In above equation, $\beta=\frac{\pi}{h}$ and also $\bar{\Phi}(\bar{x},\bar{t})$ is the spatial and time variation of the electric potential in the x-direction (Ke *et al.* 2010); V_0 is the external electric voltage (Liew *et al.* 2003). It is noted that $\bar{\Phi}(\bar{x},\bar{t})$ must satisfy the electric boundary conditions. According to Eq. (8), the electric fields can be defined as

$$\begin{aligned}E_{\bar{x}}&=-\frac{\partial\tilde{\Phi}}{\partial\bar{x}}=-\cos\left(\beta\bar{z}\right)\frac{\partial\bar{\Phi}}{\partial\bar{x}}\\ E_{\bar{z}}&=-\frac{\partial\tilde{\Phi}}{\partial\bar{z}}=\beta\sin\left(\beta\bar{z}\right)\bar{\Phi}\left(\bar{x},\bar{t}\right)-E_0,\qquad E_0=\frac{2V_0}{h_H}\end{aligned} \tag{9}$$

The strain-stress constitutive relations for face-sheets made of CNTRC are defined as (Li *et al.* 2015)

$$\begin{aligned}\sigma_{\bar{x}\bar{x}}^{f}&=E^{f}\left(\bar{z}\right)\left(\frac{\partial u_0}{\partial\bar{x}}-\bar{z}\frac{\partial^2 w_0}{\partial\bar{x}^2}+\varphi\left(\frac{\partial^2 w_0}{\partial\bar{x}^2}-\frac{\partial\phi}{\partial\bar{x}}\right)-\alpha\left(\bar{z}\right)\Delta T\right)\\ \sigma_{\bar{x}\bar{z}}^{f}&=G^{f}\left(\bar{z}\right)\frac{\partial\varphi}{\partial\bar{z}}\left(\frac{\partial w_0}{\partial\bar{x}}-\phi\right)\end{aligned} \tag{10}$$

Superscripts p and f are employed for description of properties of core and face-sheets respectively. Taking into account the voltage applied on piezoelectric core layer, the constitutive relations of the core are expressed as

$$\begin{aligned}\sigma_{\bar{x}\bar{x}}^{p}&=E^{p}\left(\frac{\partial u_0}{\partial\bar{x}}-\bar{z}\frac{\partial^2 w_0}{\partial\bar{x}^2}+\varphi\left(\frac{\partial^2 w_0}{\partial\bar{x}^2}-\frac{\partial\phi}{\partial\bar{x}}\right)-\alpha\left(\bar{z}\right)\Delta T\right)-e_{31}E_{\bar{z}}\\ \sigma_{\bar{x}\bar{z}}^{p}&=G^{p}\frac{\partial\varphi}{\partial\bar{z}}\left(\frac{\partial w_0}{\partial\bar{x}}-\phi\right)-e_{15}E_{\bar{x}}\\ D_{\bar{x}}&=e_{15}\varepsilon_{\bar{x}\bar{z}}-k_{11}E_{\bar{x}}\\ D_{\bar{z}}&=e_{31}\varepsilon_{\bar{x}\bar{x}}-k_{33}E_{\bar{z}}\end{aligned} \tag{11}$$

In which, $D_{\bar{x}}$ and $D_{\bar{z}}$ represent the electric displacement. In addition, e_{31}, e_{15} are the piezoelectric strain constants and also k_{11}, k_{33} are the dielectric constants (Liew *et al.* 2003, Rafiee *et al.* 2013). In order to extract the governing equations of motion, the Hamilton's principle is used as the following form (Komijani *et al.* 2014)

$$0=\int_0^T\left(\delta T-\delta U_s-\delta U_f+\delta W\right)d\bar{t} \tag{12}$$

Where δU_s, δU_f, δT and δW are the variations of strain energy, foundation reaction, kinetic energy and external works, respectively. Variation of strain energy δU is calculated as

$$\delta U_s=\int_0^L\int_A\left(\sigma_{\bar{x}\bar{x}}\delta\varepsilon_{\bar{x}\bar{x}}+\sigma_{\bar{x}\bar{z}}\delta\varepsilon_{\bar{x}\bar{z}}-D_{\bar{x}}E_{\bar{x}}-D_{\bar{z}}E_{\bar{z}}\right)dAd\bar{x} \tag{13}$$

Variation of kinetic energy is represented as

$$\delta T=\int_0^L\int_A\rho\left(\bar{z}\right)\left(\frac{\partial\bar{u}}{\partial\bar{t}}\frac{\partial\delta\bar{u}}{\partial\bar{t}}+\frac{\partial\bar{w}}{\partial\bar{t}}\frac{\partial\delta\bar{w}}{\partial\bar{t}}\right)dAd\bar{x} \tag{14}$$

Variations of work done by the external forces and the elastic foundation are written as (Ghorbanpour Arani *et al* .2012, Kanani *et al*. 2014, Komijani *et al.* 2014)

$$\begin{aligned}\delta W&=\int_0^L\left(F\delta u_0+Q\delta w_0+\bar{N}_{\bar{x}_0}\frac{\partial w_0}{\partial\bar{x}}\frac{\partial\delta w_0}{\partial\bar{x}}\right)d\bar{x}\\ \delta U_f&=\int_0^L\int_0^b\left(\bar{K}_w w_0\delta w_0+\bar{K}_s\frac{\partial w_0}{\partial\bar{x}}\delta\left(\frac{\partial w_0}{\partial\bar{x}}\right)\right)d\bar{y}d\bar{x}\end{aligned} \tag{15}$$

Where F and Q are the axial and transverse forces per unit length respectively and $\bar{N}_{\bar{x}_0}$ is the normal loading induced by the external magnetic potential $\bar{H}_x$, external electric potential and temperature change ΔT (Ma *et al.* 2017). Also, $\bar{K}_w$ and $\bar{K}_s$ are linear spring constant (Winkler coefficient) and shear coefficient (Pasternak coefficient) of foundation, respectively. Substituting Eqs. (4)-(7) and Eq. (9) into Eqs. (13)-(15) and consequently into Eq. (12), yields the governing equations of motions as

$$\begin{aligned}&\delta u_0:\ \frac{\partial N_{\bar{x}}}{\partial\bar{x}}+F=\bar{I}_A\frac{\partial^2 u_0}{\partial\bar{t}^2}-\bar{I}_{B1}\frac{\partial^3 w_0}{\partial\bar{t}^2\partial\bar{x}}+\bar{I}_{B2}\frac{\partial^3 w_0}{\partial\bar{t}^2\partial\bar{x}}-\bar{I}_{B2}\frac{\partial^2\phi}{\partial\bar{t}^2}\\ &\delta w_0:\ \frac{\partial^2 M_{\bar{x}}}{\partial\bar{x}^2}-\frac{\partial^2 M_{\bar{x}}^h}{\partial\bar{x}^2}+\bar{N}_{\bar{x}_0}\frac{\partial^2 w_0}{\partial\bar{x}^2}+\frac{\partial Q_{\bar{x}\bar{z}}}{\partial\bar{x}}-\bar{K}_w w_0+\bar{K}_s\frac{\partial^2 w_0}{\partial\bar{x}^2}+Q\\ &\qquad=\bar{I}_{B1}\frac{\partial^3 u_0}{\partial\bar{x}\partial\bar{t}^2}-\bar{I}_{B2}\frac{\partial^3 u_0}{\partial\bar{x}\partial\bar{t}^2}+\bar{I}_A\frac{\partial^2 w_0}{\partial\bar{t}^2}\\ &\qquad-\bar{I}_{D1}\frac{\partial^4 w_0}{\partial\bar{t}^2\partial\bar{x}^2}+2\bar{I}_{D2}\frac{\partial^4 w_0}{\partial\bar{t}^2\partial\bar{x}^2}-\bar{I}_{D3}\frac{\partial^4 w_0}{\partial\bar{t}^2\partial\bar{x}^2}\\ &\qquad-\bar{I}_{D2}\frac{\partial^3\phi}{\partial\bar{x}\partial\bar{t}^2}+\bar{I}_{D3}\frac{\partial^3\phi}{\partial\bar{x}\partial\bar{t}^2}\\ &\delta\phi:\ Q_{\bar{x}\bar{z}}-\frac{\partial M_{\bar{x}}}{\partial\bar{x}}=\bar{I}_{B2}\frac{\partial^2 u_0}{\partial\bar{t}^2}+\bar{I}_{D2}\frac{\partial^3 w_0}{\partial\bar{t}^2\partial\bar{x}}-\bar{I}_{D3}\frac{\partial^3 w_0}{\partial\bar{t}^2\partial\bar{x}}+\bar{I}_{D3}\frac{\partial^2\phi}{\partial\bar{t}^2}\\ &\delta\xi:\ \int_A\left(\cos\left(\beta\bar{z}\right)\frac{\partial\bar{D}_{\bar{x}}}{\partial\bar{x}}-\beta\sin\left(\beta\bar{z}\right)\bar{D}_{\bar{z}}\right)dA=0\end{aligned} \tag{16}$$

Where, $N_{\bar{x}_0}$ is the axial constant pretention and also $N_{\bar{x}}$, $Q_{\bar{x}\bar{z}}$, $M_{\bar{x}}$ and $M_{\bar{x}}^h$ are the resultants of forces and the moments. They are expressed as

$$\begin{aligned}N_{\bar{x}}&=\int_{-h/2}^{h/2}\sigma_{\bar{x}\bar{x}}\left(\bar{z}\right)d\bar{z}=\left(\int_{t_0}^{t_1}\sigma_{\bar{x}\bar{x}}^{f}d\bar{z}+\int_{t_1}^{t_2}\sigma_{\bar{x}\bar{x}}^{p}d\bar{z}+\int_{t_2}^{t_3}\sigma_{\bar{x}\bar{x}}^{f}d\bar{z}\right)\\ Q_{\bar{x}\bar{z}}&=\int_{-h/2}^{h/2}\frac{\partial\varphi\left(\bar{z}\right)}{\partial\bar{x}}\sigma_{\bar{x}\bar{z}}\left(\bar{z}\right)d\bar{z}=\left(\int_{t_0}^{t_1}\frac{\partial\varphi\left(\bar{z}\right)}{\partial\bar{x}}\sigma_{\bar{x}\bar{x}}^{f}d\bar{z}+\int_{t_1}^{t_2}\frac{\partial\varphi\left(\bar{z}\right)}{\partial\bar{x}}\sigma_{\bar{x}\bar{x}}^{p}d\bar{z}\right.\\ &\quad\left.+\int_{t_2}^{t_3}\frac{\partial\varphi\left(\bar{z}\right)}{\partial\bar{x}}\sigma_{\bar{x}\bar{x}}^{f}d\bar{z}\right)\\ M_{\bar{x}}&=\int_{-h/2}^{h/2}\bar{z}\sigma_{\bar{x}\bar{x}}\left(\bar{z}\right)d\bar{z}=\left(\int_{t_0}^{t_1}\bar{z}\sigma_{\bar{x}\bar{x}}^{f}d\bar{z}+\int_{t_1}^{t_2}\bar{z}\sigma_{\bar{x}\bar{x}}^{p}d\bar{z}+\int_{t_2}^{t_3}\bar{z}\sigma_{\bar{x}\bar{x}}^{f}d\bar{z}\right)\\ M_{\bar{x}}^{h}&=\int_{-h/2}^{h/2}\varphi\left(\bar{z}\right)\sigma_{\bar{x}\bar{x}}\left(\bar{z}\right)d\bar{z}=\left(\int_{t_0}^{t_1}\varphi\left(\bar{z}\right)\sigma_{\bar{x}\bar{x}}^{f}d\bar{z}+\int_{t_1}^{t_2}\varphi\left(\bar{z}\right)\sigma_{\bar{x}\bar{x}}^{p}d\bar{z}+\right.\\ &\quad\left.\int_{t_2}^{t_3}\varphi\left(\bar{z}\right)\sigma_{\bar{x}\bar{x}}^{f}d\bar{z}\right)\end{aligned} \tag{17}$$

The integration constants presented in Eq. (16) can be presented as

$$\begin{aligned}
&\bar{I}_A = \int_{-H/2}^{H/2} \rho(\bar{z})\, d\bar{z} \\
&\begin{Bmatrix} \bar{I}_{B1} \\ \bar{I}_{B2} \end{Bmatrix} = \int_{-H/2}^{H/2} \begin{Bmatrix} \bar{z} \\ \varphi(\bar{z}) \end{Bmatrix} \rho(\bar{z})\, d\bar{z} \\
&\begin{Bmatrix} \bar{I}_{D1} \\ \bar{I}_{D2} \\ \bar{I}_{D3} \end{Bmatrix} = \int_{-H/2}^{H/2} \begin{Bmatrix} \bar{z}^2 \\ \bar{z}\varphi(\bar{z}) \\ \varphi(\bar{z})^2 \end{Bmatrix} \rho(\bar{z})\, d\bar{z}
\end{aligned} \tag{18}$$

In according to nonlocal strain gradient theory (Li and Hu 2016), the constitutive relations are expressed as

$$\begin{aligned}
&\left(1-(\bar{e}_0\bar{a})^2\nabla^2\right)\sigma_{\bar{x}\bar{x}} = E(z)\left(1-\bar{l}_m^2\nabla^2\right)\varepsilon_{\bar{x}\bar{x}} - E(\bar{z})\alpha(\bar{z})\Delta T - e_{31}E_{\bar{z}} \\
&\left(1-(\bar{e}_0\bar{a})^2\nabla^2\right)\sigma_{\bar{x}\bar{z}} = G(z)\left(1-\bar{l}_m^2\nabla^2\right)\varepsilon_{\bar{x}\bar{z}} - e_{15}E_{\bar{x}} \\
&\left(1-(\bar{e}_0\bar{a})^2\nabla^2\right)D_{\bar{x}} = e_{15}\left(1-\bar{l}_m^2\nabla^2\right)\varepsilon_{\bar{x}\bar{z}} - k_{11}E_{\bar{x}} \\
&\left(1-(\bar{e}_0\bar{a})^2\nabla^2\right)D_{\bar{z}} = e_{31}\left(1-\bar{l}_m^2\nabla^2\right)\varepsilon_{\bar{x}\bar{x}} - k_{33}E_{\bar{z}}
\end{aligned} \tag{19}$$

In above equation, $\nabla^2 = \partial^2/\partial\bar{x}^2$ is the Laplacian operator, $\bar{e}_0\bar{a}$ represents the nonlocal parameter to consider the significance of nonlocal elastic stress field, and $\bar{l}_m$ is the strain gradient length scale parameter. In present structure, the nonlocal strain gradient constitutive relation in Eq. (19) can be written in an explicit form as follows

$$\begin{aligned}
&\left(1-(\bar{e}_0\bar{a})^2\nabla^2\right)\sigma_{\bar{x}\bar{x}} = \left(1-\bar{l}_m^2\nabla^2\right)E(\bar{z})\left[\frac{\partial u_0}{\partial\bar{x}} - \bar{z}\frac{\partial^2 w_0}{\partial\bar{x}^2}\right. \\
&\left.+\varphi\left(\frac{\partial^2 w_0}{\partial\bar{x}^2} - \frac{\partial\phi}{\partial\bar{x}}\right)\right] - E(\bar{z})\alpha(\bar{z})\Delta T - e_{31}\left(\beta\sin(\beta\bar{z})\bar{\Phi}(\bar{x},\bar{t}) - E_0\right) \\
&\left(1-(\bar{e}_0\bar{a})^2\nabla^2\right)\sigma_{\bar{x}\bar{z}} = \left(1-\bar{l}_m^2\nabla^2\right)G(\bar{z})\left[\frac{\partial\varphi}{\partial\bar{z}}\left(\frac{\partial w_0}{\partial\bar{x}} - \phi\right)\right] \\
&\quad + e_{15}\left(\cos(\beta\bar{z})\frac{\partial\bar{\Phi}}{\partial\bar{x}}\right) \\
&\left(1-(\bar{e}_0\bar{a})^2\nabla^2\right)D_{\bar{x}} = e_{15}\left(1-\bar{l}_m^2\nabla^2\right)\left[\frac{\partial\varphi}{\partial\bar{z}}\left(\frac{\partial w_0}{\partial\bar{x}} - \phi\right)\right] + \\
&\quad k_{11}\left(\cos(\beta\bar{z})\frac{\partial\bar{\Phi}}{\partial\bar{x}}\right) \\
&\left(1-(\bar{e}_0\bar{a})^2\nabla^2\right)D_{\bar{z}} = e_{31}\left(1-\bar{l}_m^2\nabla^2\right)\left[\frac{\partial u_0}{\partial\bar{x}} - \bar{z}\frac{\partial^2 w_0}{\partial\bar{x}^2}\right. \\
&\left.+\varphi\left(\frac{\partial^2 w_0}{\partial\bar{x}^2} - \frac{\partial\phi}{\partial\bar{x}}\right)\right] - k_{33}\left(\beta\sin(\beta\bar{z})\bar{\Phi}(\bar{x},\bar{t}) - E_0\right)
\end{aligned} \tag{20}$$

Based on defined mechanical and electrical relations, the resultant of them can be calculated as follows

$$\begin{aligned}
&\left(1-(\bar{e}_0\bar{a})^2\nabla^2\right)N_{\bar{x}\bar{x}} = \left(1-\bar{l}_m^2\nabla^2\right) \\
&\left[\bar{A}_{\bar{x}}\frac{\partial u_0}{\partial\bar{x}} - \bar{B}_{\bar{x}1}\frac{\partial^2 w_0}{\partial\bar{x}^2} + \bar{B}_{\bar{x}2}\left(\frac{\partial^2 w_0}{\partial\bar{x}^2} - \frac{\partial\phi}{\partial\bar{x}}\right)\right] - \bar{N}^T - \bar{N}^E \\
&\left(1-(\bar{e}_0\bar{a})^2\nabla^2\right)M_{\bar{x}\bar{x}} = \left(1-\bar{l}_m^2\nabla^2\right) \\
&\left[\bar{B}_{\bar{x}1}\frac{\partial u_0}{\partial\bar{x}} - \bar{D}_{\bar{x}1}\frac{\partial^2 w_0}{\partial\bar{x}^2} + \bar{D}_{\bar{x}2}\left(\frac{\partial^2 w_0}{\partial\bar{x}^2} - \frac{\partial\phi}{\partial\bar{x}}\right)\right] - \bar{M}^{T1} - \bar{M}^{E1} \\
&\left(1-(\bar{e}_0\bar{a})^2\nabla^2\right)M_{\bar{x}\bar{x}}^h = \left(1-\bar{l}_m^2\nabla^2\right) \\
&\left[\bar{B}_{\bar{x}2}\frac{\partial u_0}{\partial\bar{x}} - \bar{D}_{\bar{x}2}\frac{\partial^2 w_0}{\partial\bar{x}^2} + \bar{D}_{\bar{x}3}\left(\frac{\partial^2 w_0}{\partial\bar{x}^2} - \frac{\partial\phi}{\partial\bar{x}}\right)\right] - \bar{M}^{T2} - \bar{M}^{E2} \\
&\left(1-(\bar{e}_0\bar{a})^2\nabla^2\right)Q_{\bar{x}\bar{z}} = \left(1-\bar{l}_m^2\nabla^2\right)\bar{A}_{\bar{x}\bar{z}}\left[\frac{\partial w_0}{\partial\bar{x}} - \phi\right] + \\
&\int_A e_{15}\left(\cos(\beta\bar{z})\frac{\partial\bar{\Phi}}{\partial\bar{x}}\right)dA \\
&\left(1-(\bar{e}_0\bar{a})^2\nabla^2\right)\bar{D}_{\bar{x}} = \left(1-\bar{l}_m^2\nabla^2\right)e_{15}\frac{\partial\varphi}{\partial\bar{z}}\left[\frac{\partial w_0}{\partial\bar{x}} - \phi\right] - \\
&k_{xx}\left(\cos(\beta\bar{z})\frac{\partial\bar{\Phi}}{\partial\bar{x}}\right) \\
&\left(1-(\bar{e}_0\bar{a})^2\nabla^2\right)\bar{D}_{\bar{z}} = \left(1-\bar{l}_m^2\nabla^2\right) \\
&e_{31}\left[\frac{\partial u_0}{\partial\bar{x}} - \bar{z}\frac{\partial^2 w_0}{\partial\bar{x}^2} + \varphi(\bar{z})\left(\frac{\partial w_0}{\partial\bar{x}} - \phi\right)\right] - \alpha(\bar{z})\Delta T + \\
&k_{\bar{z}\bar{z}}\left(\beta\sin(\beta\bar{z})\bar{\Phi}(\bar{x},\bar{t}) - E_0\right)
\end{aligned} \tag{21}$$

Where superscripts T and E represent thermal and electrical loads and $\bar{N}^T$, $\bar{N}^E$, $\bar{M}^{T1}, \bar{M}^{T2}, \bar{M}^{E1}$ and $\bar{M}^{E2}$ are calculated as

$$\begin{aligned}
&\begin{pmatrix} \bar{N}^T \\ \bar{N}^E \end{pmatrix} = \int_{-H/2}^{H/2} \begin{pmatrix} E(\bar{z})\alpha(\bar{z})\Delta T \\ e_{31}\left(\beta\sin(\beta\bar{z})\bar{\Phi}(\bar{x},\bar{t}) - E_0\right) \end{pmatrix} d\bar{z} \\
&\begin{pmatrix} \bar{M}^{T1} \\ \bar{M}^{E1} \end{pmatrix} = \int_{-H/2}^{H/2} \begin{pmatrix} E(\bar{z})\alpha(\bar{z})\Delta T \\ e_{31}\left(\beta\sin(\beta\bar{z})\bar{\Phi}(\bar{x},\bar{t}) - E_0\right) \end{pmatrix} \bar{z}\, d\bar{z} \\
&\begin{pmatrix} \bar{M}^{T2} \\ \bar{M}^{E2} \end{pmatrix} = \int_{-H/2}^{H/2} \begin{pmatrix} E(\bar{z})\alpha(\bar{z})\Delta T \\ e_{31}\left(\beta\sin(\beta\bar{z})\bar{\Phi}(\bar{x},\bar{t}) - E_0\right) \end{pmatrix} \varphi(\bar{z})\, d\bar{z}
\end{aligned} \tag{22}$$

It is noted that, A_x, B_x and D_x in Eq. (21) are the stretching stiffness, stretching-bending coupling stiffness and bending stiffness coefficients , respectively, which can be obtained as

$$\begin{aligned}
&\bar{A}_{\bar{x}} = \int_{-H/2}^{H/2} E(\bar{z})\, dA \\
&\begin{Bmatrix} \bar{B}_{\bar{x}1} \\ \bar{B}_{\bar{x}2} \end{Bmatrix} = \int_{-H/2}^{H/2} \begin{Bmatrix} \bar{z} \\ \varphi(\bar{z}) \end{Bmatrix} E(\bar{z})\, d\bar{z} \\
&\begin{Bmatrix} \bar{D}_{\bar{x}1} \\ \bar{D}_{\bar{x}2} \\ \bar{D}_{\bar{x}3} \end{Bmatrix} = \int_{-H/2}^{H/2} \begin{Bmatrix} \bar{z}^2 \\ \bar{z}\varphi(\bar{z}) \\ \varphi(\bar{z})^2 \end{Bmatrix} E(\bar{z})\, d\bar{z}
\end{aligned} \tag{23}$$

To obtain the equations of motion, Eq. (21) should be substituted into Eq. (16). Therefore, four coupled equations of motion are obtained:

$$\delta u_0 : \left(1-\bar{l}_m^{\,2}\nabla^2\right)\left(\bar{A}_{\bar{x}}\frac{\partial^2 u_0}{\partial \bar{x}^2}-\bar{B}_{\bar{x}1}\frac{\partial^3 w_0}{\partial \bar{x}^3}+\bar{B}_{\bar{x}2}\left(\frac{\partial^3 w_0}{\partial \bar{x}^3}-\frac{\partial^2 \phi}{\partial \bar{x}^2}\right)\right)+$$
$$\left(1-\left(\bar{e}_0\bar{a}\right)^2\nabla^2\right)F=\left(1-\left(\bar{e}_0\bar{a}\right)^2\nabla^2\right)$$
$$\left(\bar{I}_A\frac{\partial^2 u_0}{\partial \bar{t}^2}-\bar{I}_{B1}\frac{\partial^3 w_0}{\partial \bar{t}^2\partial \bar{x}}+\bar{I}_{B2}\frac{\partial^3 w_0}{\partial \bar{t}^2\partial \bar{x}}-\bar{I}_{B2}\frac{\partial^2 \phi}{\partial \bar{t}^2}\right)$$

$$\delta w_0 : -\left(1-\bar{l}_m^{\,2}\nabla^2\right)\left(\bar{B}_{\bar{x}2}\frac{\partial^3 u_0}{\partial \bar{x}^3}-\bar{D}_{\bar{x}2}\frac{\partial^4 w_0}{\partial \bar{x}^4}+\bar{D}_{\bar{x}3}\frac{\partial^4 w_0}{\partial \bar{x}^4}-\bar{D}_{\bar{x}3}\frac{\partial^3 \phi}{\partial \bar{x}^3}\right)$$
$$+\left(1-\bar{l}_m^{\,2}\nabla^2\right)\left(\bar{B}_{\bar{x}1}\frac{\partial^3 u_0}{\partial \bar{x}^3}-\bar{D}_{\bar{x}1}\frac{\partial^4 w_0}{\partial \bar{x}^4}+\bar{D}_{\bar{x}2}\frac{\partial^4 w_0}{\partial \bar{x}^4}-\bar{D}_{\bar{x}2}\frac{\partial^3 \phi}{\partial \bar{x}^3}\right)+$$
$$\bar{M}^{E1}\frac{\partial^2 \bar{\Phi}}{\partial \bar{x}^2}-\bar{M}^{E2}\frac{\partial^2 \bar{\Phi}}{\partial \bar{x}^2}-\bar{N}^T\frac{\partial^2 w_0}{\partial \bar{x}^2}+\bar{N}^E\frac{\partial^2 w_0}{\partial \bar{x}^2}-\bar{K}_w w_0+\bar{K}_s\frac{\partial^2 w_0}{\partial \bar{x}^2}+$$
$$\bar{A}_{\bar{x}\bar{z}1}\left(1-\bar{l}_m^{\,2}\nabla^2\right)\frac{\partial^2 w_0}{\partial \bar{x}^2}-\bar{A}_{\bar{x}\bar{z}1}\left(1-\bar{l}_m^{\,2}\nabla^2\right)\frac{\partial \phi}{\partial \bar{x}}+\bar{A}_{\bar{x}\bar{z}2}\frac{\partial^2 \bar{\Phi}}{\partial \bar{x}^2}+E^{15}\frac{\partial^2 \bar{\Phi}}{\partial \bar{x}^2}=$$
$$+\left(1-\left(\bar{e}_0\bar{a}\right)^2\nabla^2\right)\left(\bar{I}_{B1}\frac{\partial^3 u_0}{\partial \bar{x}\partial \bar{t}^2}-\bar{I}_{B2}\frac{\partial^3 u_0}{\partial \bar{x}\partial \bar{t}^2}+\bar{I}_A\frac{\partial^2 w_0}{\partial \bar{t}^2}-\bar{I}_{D1}\frac{\partial^4 w_0}{\partial \bar{t}^2\partial \bar{x}^2}\right. \quad (24)$$
$$\left.+2\bar{I}_{D2}\frac{\partial^4 w_0}{\partial \bar{t}^2\partial \bar{x}^2}-\bar{I}_{D3}\frac{\partial^4 w_0}{\partial \bar{t}^2\partial \bar{x}^2}-\bar{I}_{D2}\frac{\partial^3 \phi}{\partial \bar{x}\partial \bar{t}^2}+\bar{I}_{D3}\frac{\partial^3 \phi}{\partial \bar{x}\partial \bar{t}^2}\right)$$

$$\delta\phi : \left(1-\bar{l}_m^{\,2}\nabla^2\right)\bar{A}_{\bar{x}\bar{z}1}\left(\frac{\partial w_0}{\partial \bar{x}}-\phi\right)+E^{15}\frac{\partial \bar{\Phi}}{\partial \bar{x}}-\left(1-\bar{l}_m^{\,2}\nabla^2\right)\left(\bar{B}_{\bar{x}2}\frac{\partial^2 u_0}{\partial \bar{x}^2}-\right.$$
$$\left.\bar{D}_{\bar{x}2}\frac{\partial^3 w_0}{\partial \bar{x}^3}+\bar{D}_{\bar{x}3}\frac{\partial^3 w_0}{\partial \bar{x}^3}-\bar{D}_{\bar{x}3}\frac{\partial^2 \phi}{\partial \bar{x}^2}\right)-E_3^{\,13}\frac{\partial \bar{\Phi}}{\partial \bar{x}}=+\left(1-\left(\bar{e}_0\bar{a}\right)^2\nabla^2\right)$$
$$\left(\bar{I}_{B2}\frac{\partial^2 u_0}{\partial \bar{t}^2}+\bar{I}_{D2}\frac{\partial^3 w_0}{\partial \bar{t}^2\partial \bar{x}}-\bar{I}_{D3}\frac{\partial^3 w_0}{\partial \bar{t}^2\partial \bar{x}}+\bar{I}_{D3}\frac{\partial^2 \phi}{\partial \bar{t}^2}\right)$$

$$\delta\bar{\Phi} : \left(1-\bar{l}_m^{\,2}\nabla^2\right)\left(E^{15}+E_3^{\,13}\right)\left(\frac{\partial^2 w_0}{\partial \bar{x}^2}-\frac{\partial \phi}{\partial \bar{x}}\right)-\left(1-\bar{l}_m^{\,2}\nabla^2\right)E_2^{31}\frac{\partial^2 w_0}{\partial \bar{x}^2}$$
$$-k_{xx}\frac{\partial^2 \bar{\Phi}}{\partial \bar{x}^2}+k_{zz}\bar{\Phi}=0$$

In which, E^{15}, E_2^{31}, E_3^{31}, $k_{\bar{x}\bar{x}}$ and $k_{\bar{z}\bar{z}}$ are calculated as the following form

$$E^{15}=\int_A e_{15}\frac{\partial \varphi(\bar{z})}{\partial \bar{z}}\cos(\beta\bar{z})\,dA$$
$$E_2^{31}=\int_A \beta e_{31}\bar{z}\sin(\beta\bar{z})\,dA$$
$$E_2^{31}=\int_A \beta e_{31}\varphi(\bar{z})\sin(\beta\bar{z})\,dA \quad (25)$$
$$k_{\bar{x}\bar{x}}=\int_A k_{11}\cos^2(\beta\bar{z})\,dA$$
$$k_{\bar{z}\bar{z}}=\int_A k_{33}\beta^2\cos^2(\beta\bar{z})\,dA$$

Regarding to dimensionless variables defined as the following form

$$x=\frac{\bar{x}}{L},\quad w=\frac{w_0}{h},\quad ,\mu_1=\frac{\bar{l}_m}{L},\quad \mu_2=\frac{\bar{e}_0\bar{a}}{L},\quad t=\frac{\bar{t}}{T_0},$$
$$T_0=L\sqrt{\frac{\bar{I}_A}{\bar{A}_{\bar{x}}}},\ R=\frac{h}{L},\quad A_{xz}=\frac{\bar{A}_{\bar{x}\bar{z}}}{\bar{A}_{\bar{x}}},$$
$$\left[I_{D1}\quad I_{D2}\quad I_{D3}\right]=\frac{\left[\bar{I}_{D1}\quad \bar{I}_{D2}\quad \bar{I}_{D3}\right]}{\bar{I}_A L^2},\ k_{zz}=\frac{\bar{k}_{\bar{z}\bar{z}}\Phi_0^2}{\bar{A}_{\bar{x}}}$$
$$\left[D_{x1}\quad D_{x2}\quad D_{x3}\right]=\frac{\left[\bar{D}_{\bar{x}1}\quad \bar{D}_{\bar{x}2}\quad \bar{D}_{\bar{x}3}\right]}{\bar{A}_{\bar{x}}L^2},\quad N^T=\frac{\bar{N}^T}{\bar{A}_{\bar{x}}}, \quad (26)$$
$$N^E=\frac{\bar{N}^E}{\bar{A}_{\bar{x}}},M^{E1}=\frac{\bar{M}^{E1}\Phi_0}{\bar{A}_{\bar{x}}h},\quad M^{E2}=\frac{\bar{M}^{E2}\Phi_0}{\bar{A}_{\bar{x}}h},\quad \Phi_0=\frac{\bar{A}_{\bar{x}}}{e_{15}},$$
$$\Phi=\frac{\bar{\Phi}}{\Phi_0},E^{15}=\frac{\bar{E}^{15}\Phi_0}{\bar{A}_{\bar{x}}h},\quad E_{2\ and\ 3}^{31}=\frac{\bar{E}_{2and3}^{31}\Phi_0}{\bar{A}_{\bar{x}}h},\quad K_w=\frac{\bar{K}_w L^2}{\bar{A}_{\bar{x}}},$$
$$K_s=\frac{\bar{K}_s}{\bar{A}_{\bar{x}}},\ \left[D_{x1}\quad D_{x2}\quad D_{x3}\right]=\frac{\left[\bar{B}_{\bar{x}1}\quad \bar{B}_{\bar{x}2}\right]}{\bar{A}_{\bar{x}}L},\ k_{xx}=\frac{\bar{k}_{\bar{x}\bar{x}}\Phi_0^2}{\bar{A}_{\bar{x}}h^2},$$

The final dimensionless equations of motion are obtained as

$$\delta u : \left(1-\mu_1^{\,2}\nabla^2\right)\left(\frac{\partial^2 u}{\partial x^2}-B_{x1}\frac{\partial^3 w}{\partial x^3}+B_{x2}\left(\frac{\partial^3 w}{\partial x^3}-\frac{\partial^2 \phi}{\partial x^2}\right)\right)+\left(1-\mu_2^{\,2}\nabla^2\right)F$$
$$=\left(1-\mu_2^{\,2}\nabla^2\right)\left(I_A\frac{\partial^2 u}{\partial t^2}-I_{B1}\frac{\partial^3 w}{\partial t^2\partial x}+I_{B2}\frac{\partial^3 w}{\partial t^2\partial x}-I_{B2}\frac{\partial^2 \phi}{\partial t^2}\right) \quad (27)$$

$$\delta w : -\left(1-\mu_1^{\,2}\nabla^2\right)\left(B_{x2}\frac{\partial^3 u}{\partial x^3}-D_{x2}\frac{\partial^4 w}{\partial x^4}+D_{x3}\frac{\partial^4 w}{\partial x^4}-D_{x3}\frac{1}{R}\frac{\partial^3 \phi}{\partial x^3}\right)+$$
$$\left(1-\mu_1^{\,2}\nabla^2\right)\left(B_{x1}\frac{\partial^3 u}{\partial x^3}-D_{x1}\frac{\partial^4 w}{\partial x^4}+D_{x2}\frac{\partial^4 w}{\partial x^4}-D_{x2}\frac{1}{R}\frac{\partial^3 \phi}{\partial x^3}\right)$$
$$+M^{E1}\frac{\partial^2 \Phi}{\partial x^2}-M^{E2}\frac{\partial^2 \Phi}{\partial x^2}-N^T\frac{\partial^2 w}{\partial x^2}+N^E\frac{\partial^2 w}{\partial x^2}-K_w w$$
$$+K_s\frac{\partial^2 w}{\partial x^2}-K_{nl}w^3+A_{xz}\left(1-\mu_1^{\,2}\nabla^2\right)\frac{\partial^2 w}{\partial x^2}-A_{xz}\left(1-\mu_1^{\,2}\nabla^2\right)\frac{1}{R}\frac{\partial \phi}{\partial x}$$
$$+E^{15}\frac{\partial^2 \Phi}{\partial x^2}+A_{xz2}\frac{\partial^2 \Phi}{\partial x^2}=\left(1-\mu_2^{\,2}\nabla^2\right)\left(I_{B1}\frac{\partial^3 u}{\partial x\partial t^2}-I_{B2}\frac{\partial^3 u}{\partial x\partial t^2}+\frac{\partial^2 w}{\partial t^2}\right.$$
$$\left.-I_{D1}\frac{\partial^4 w}{\partial t^2\partial x^2}+2I_{D2}\frac{\partial^4 w}{\partial t^2\partial x^2}-I_{D3}\frac{\partial^4 w}{\partial t^2\partial x^2}-I_{D2}\frac{1}{R}\frac{\partial^3 \phi}{\partial x\partial t^2}+I_{D3}\frac{1}{R}\frac{\partial^3 \phi}{\partial x\partial t^2}\right)$$

$$\delta\phi : \left(1-\mu_1^{\,2}\nabla^2\right)A_{xz}\left(\frac{\partial w}{\partial x}-\phi\right)+E^{15}\frac{\partial \Phi}{\partial x}-E_3^{\,13}\frac{\partial \Phi}{\partial x}$$
$$-\left(1-\mu_1^{\,2}\nabla^2\right)\left(B_{x2}\frac{\partial^2 u}{\partial x^2}-D_{x2}\frac{\partial^3 w}{\partial x^3}+D_{x3}\frac{\partial^3 w}{\partial x^3}-D_{x3}\frac{1}{R}\frac{\partial^2 \phi}{\partial x^2}\right)=$$
$$+\left(1-\mu_2^{\,2}\nabla^2\right)\left(I_{D2}\frac{\partial^3 w}{\partial t^2\partial x}-I_{D3}\frac{\partial^3 w}{\partial t^2\partial x}+I_{D3}\frac{\partial^2 \phi}{\partial t^2}\right)$$

$$\delta\Phi : \left(1-\mu_1^{\,2}\nabla^2\right)\left(E^{15}+E_3^{\,13}\right)\left(\frac{\partial^2 w}{\partial x^2}-\frac{1}{R}\frac{\partial \phi}{\partial x}\right)-\left(1-\mu_1^{\,2}\nabla^2\right)E_2^{31}\frac{\partial^2 w}{\partial x^2}$$
$$-k_{xx}\frac{\partial^2 \Phi}{\partial x^2}+k_{zz}\frac{1}{R^2}\Phi=0$$

4. External magnetic field

The Maxwell's equation is expressed as

$$\bar{J}=\nabla\times\vec{\bar{h}},$$
$$\nabla\times\vec{\bar{e}}=-\eta.\frac{\partial\vec{\bar{h}}}{\partial t},$$
$$div\,\vec{\bar{h}}=0, \quad (28)$$
$$\bar{e}=-\eta.\left(\frac{\partial\vec{\bar{U}}}{\partial t}\times\vec{\bar{H}}\right),$$
$$\vec{\bar{h}}=\nabla\times\left(\vec{\bar{U}}\times\vec{\bar{H}}\right),$$

In above equations, $\vec{\bar{h}}$ is the disturbing vectors of magnetic field, $\vec{\bar{J}}$ presents the current density, $\vec{e}$ represents the strength vectors of electric field and $\vec{\bar{U}}$ characterizes the vector of displacement. In addition, Hamilton arithmetic operator (∇) is $\nabla=\frac{\partial}{\partial\bar{x}}\bar{\imath}+\frac{\partial}{\partial\bar{x}}\bar{\jmath}+\frac{\partial}{\partial\bar{x}}\bar{k}$. The magnetic permeability is indicated by η. Herein, the longitudinal magnetic field vector applying on the carbon nanotube is specified as $\vec{H}=(H_{\bar{x}},0,0)$. If the displacement vector is defined as U = U (u, v, w), hence

Table 1 The material properties of the constituent material of the sandwich FG beam (Ke *et al.* 2010, Rafiee *et al*. 2013, Schoeftner *et al.* 2016)

materials	Young's modulus (GP)	Expansion coefficient(1/C°)	e_{31}	e_{15}	d_{31}	k_{11}	k_{33}
piezoelectric	63	0.9e(-6)	-4.1	14.1	2.54e(-10)	5.841e-9	7.124e-9
CNT	5.65e+3	3.4584e(-6)					

$$\vec{\bar{h}} = \nabla \times \left(\vec{\bar{U}} \times \vec{\bar{H}}\right) = -\bar{H}_x \left(\frac{\partial v}{\partial \bar{y}} + \frac{\partial w}{\partial \bar{z}}\right)\bar{i} + \bar{H}_x \frac{\partial v}{\partial \bar{x}}\bar{j} + \bar{H}_x \frac{\partial w}{\partial \bar{x}}\bar{k}$$
$$\vec{\bar{J}} = \nabla \times \vec{\bar{h}} = \bar{H}_{\bar{x}} \left(-\frac{\partial^2 v}{\partial \bar{x}\partial \bar{z}} + \frac{\partial^2 w}{\partial \bar{x}\partial \bar{y}}\right)\bar{i} - \bar{H}_x \left(\frac{\partial^2 v}{\partial \bar{y}\partial \bar{z}} + \frac{\partial^2 w}{\partial \bar{x}^2} + \frac{\partial^2 w}{\partial \bar{z}^2}\right)\bar{j} + \bar{H}_x \left(\frac{\partial^2 v}{\partial \bar{x}^2} + \frac{\partial^2 v}{\partial \bar{y}^2} + \frac{\partial^2 w}{\partial \bar{y}\partial \bar{z}}\right)\bar{k} \quad (29)$$

Therefore, the components of the Lorentz force in $\bar{x}$, $\bar{y}$ and $\bar{z}$ directions are specified by the following form

$$f_{\bar{x}} = 0$$
$$f_{\bar{y}} = \eta \bar{H}_x^2 \left(\frac{\partial^2 v}{\partial \bar{x}^2} + \frac{\partial^2 v}{\partial \bar{y}^2} + \frac{\partial^2 w}{\partial \bar{y}\partial \bar{z}}\right), \quad (30)$$
$$f_{\bar{z}} = \eta \bar{H}_x^2 \left(\frac{\partial^2 w}{\partial \bar{x}^2} + \frac{\partial^2 w}{\partial \bar{y}^2} + \frac{\partial^2 v}{\partial \bar{y}\partial \bar{z}}\right),$$

According to the defined displacement field in Eq. (3) and with attention to Eq. (30), only Lorentz force which applied on the carbon nano-tube embedded in sandwich nano-beam is specified as

$$f_z = \eta \bar{H}_x^2 \left(\frac{\partial^2 w_0}{\partial \bar{x}^2}\right) \quad (31)$$

5. Wave propagation analysis

In order to Wave propagation analysis in sandwich nano-beam, the harmonic solution is considered for Eq. (27) as the following form (Ghorbanpour Arani *et al.* 2014)

$$d(x,t) = d_0 e^{i(kx-\omega t)}, \quad d_0 = \bar{u}, \bar{w}, \bar{\phi}, \bar{\varphi} \quad (32)$$

In above equation, k and ω are wave number and frequency, respectively (Ghorbanpour Arani *et al.* 2016, Ghorbanpour Arani *et al.* 2015). Consequently, replacing Eq. (32) into Eq. (27) produces the following matrix equations for high order shear deformation sandwich nano-beam

$$\begin{bmatrix} C_{11} & C_{12} & C_{13} & C_{14} \\ C_{21} & C_{22} & C_{23} & C_{24} \\ C_{31} & C_{32} & C_{33} & C_{34} \\ C_{41} & C_{42} & C_{43} & C_{44} \end{bmatrix} \begin{bmatrix} \bar{u} \\ \bar{w} \\ \bar{\phi} \\ \bar{\varphi} \end{bmatrix} e^{i(kx-\omega t)} = 0 \quad (33)$$

In which, $C_{ij,(i,j=1,\ldots,4)}$ are calculated as following form

$$C_{11} = c_1 k^2 + c_2 \omega^2, \qquad c_1 = 1 + k^2 \mu_1^2, \; c_2 = 1 + k^2 \mu_2^2$$
$$C_{12} = -c_1 i k^3 B_{x2} - c_2 i k \omega^2 I_{d1} + c_2 i k \omega^2 I_{d2}$$
$$C_{13} = \frac{1}{R}\left(c_1 B_{x2} k^2 - c_2 I_{d2} \omega^2\right) \quad (34)$$
$$C_{14} = 0$$

$$C_{21} = -c_1 i k^3 B_{x1} + c_1 i k^3 B_{x2} + c_2 i k \omega^2 I_{d1} - c_2 i k \omega^2 I_{d2}$$
$$C_{22} = -c_1 k^4 D_{x1} + 2c_1 k^4 D_{x2} - c_1 k^4 D_{x3} - c_1 k^2 A_{xz1} + c_2 \omega^2 - c_2 k^2 \omega^2 I_{d1} - 2c_2 k^2 \omega^2 I_{d2} + 2c_2 k^2 \omega^2 I_{d3} + c_2 k^2 \left(N_0 + N_t + N_e\right) - c_2 \left(K_w + K_s k^2 + H_x k^2\right)$$
$$C_{23} = \frac{1}{R}\left(c_1 i k^3 D_{x2} - c_1 i k^3 D_{x3} - c_1 i k A_{xz1} - c_2 i k \omega^2 I_{d2} + c_2 i k \omega^2 I_{d3}\right)$$
$$C_{24} = E_{15} i k - E_{31} i k$$
$$C_{31} = c_1 B_{x2} k^2 - c_2 I_{d2} \omega^2$$
$$C_{32} = c_1 k i A_{xz1} - c_1 k^3 i D_{x2} + c_1 k^3 i D_{x3} + c_2 i \omega^2 I_{d2} - c_2 i k \omega^2 I_{d3}$$
$$C_{33} = -c_1 A_{xz1} - \frac{c_1 k^2 D_{x3}}{R} + \frac{c_2 I_{d3} \omega^2}{R}$$
$$C_{34} = c_1 E^{15} k^2 - c_2 E_{31}^3 i k$$
$$C_{41} = 0$$
$$C_{42} = -\left(c_1 E^{15} k^2 + c_1 E_3^{31} k^2 - c_1 E_2^{31} k^2\right)$$
$$C_{43} = -\frac{c_1}{R}\left(E_{15} i k + E_3^{31} i k\right)$$
$$C_{44} = X_{11} k^2 + \frac{X_{33}}{R^2}$$

In order to obtain a nontrivial solution, it is necessary to set the determinant of the coefficient matrix in Eq. (33) equal to zero (Ghorbanpour Arani *et al*. 2014, Ghorbanpour Arani *et al*. 2016, Ghorbanpour Arani *et al*. 2015). The cut-off frequency of the sandwich nano-beam can be calculated by setting $k \to \infty$. In other words, at a certain frequency, the flexural wave number tends to infinite and the corresponding wave velocity tends to zero at that frequency, this frequency is called as cut-off frequency (Ghorbanpour Arani *et al*. 2015). Furthermore, the complex phase velocity C of flexural waves can be obtained as

$$C = \frac{\omega}{k} \quad (35)$$

6. Numerical results and discussion

In this section, a parametric study is implemented to

indicate the effects of applied voltage, the magnetic field, the Pasternak foundation, small scale parameters and the volume fraction on wave propagation characteristics in sandwich nano-beam with CNTRC face-sheets. The material properties of the sandwich nano-beam are presented in Table 1. To demonstrate the accuracy of the equations derived in present study, comparison was done between our results and other results existing in other references. Table 2 presented the comparison between results obtained by DQM in present study and results calculated by exact solution and Multiple Times Scales method for Euler-Bernoulli beams in other references (Gheshlaghi and Hasheminejad 2011, Nayfeh and Mook 2008).

According to these comparisons it is deduced that the present results are in good agreement with the obtained results presented in aforementioned references represented in Table 2. Therefore it is concluded that the extracted governing equation in present study have acceptable accuracy. It is worthy noted that an exact comparison of the results obtained for wave propagation in this work with existing experimental results is impossible. However, the present work could be partially validated based on investigation presented by Li *et al*. (2015; 2016). As can be seen in Fig. 2, in both study (present investigation and works accomplished by Li *et al*.), small scale have the same effects on phase velocity behavior of wave propagation. In aforementioned results the parameter values that are used to obtain the results are equal to $\mu_2 = 0.2$ and $\mu_1 = 0.1$ for nonlocal strain gradient theory (NSGT); $\mu_1 = \mu_2 = 0$ for classical elasticity theory (CET); $\mu_2 = 0$ and $\mu_1 = 0.1$ for strain gradient theory (SGT); $\mu_2 = 0.2$ and $\mu_1 = 0$ for nonlocal elasticity theory (NET); and also $V_{CN}^* = 0.17$, $\eta = 0.142$, $\bar{H}_x = 1E+07$, $E_0 = 3.3E-03$.

Real and imaginary parts of non-dimensional phase velocity of the wave propagation versus non-dimensional wave number are indicated in Fig. 3 for various non-dimensional nonlocal parameters. It can be seen that the real part is starting to increase when the imaginary part becomes zero. This fact shows that imaginary part has damping characteristic for wave propagation of the sandwich nano-beam. In addition, increasing nonlocal parameter causes that the phase velocity increases/ decreases in very small wave numbers range/in large wave numbers range.

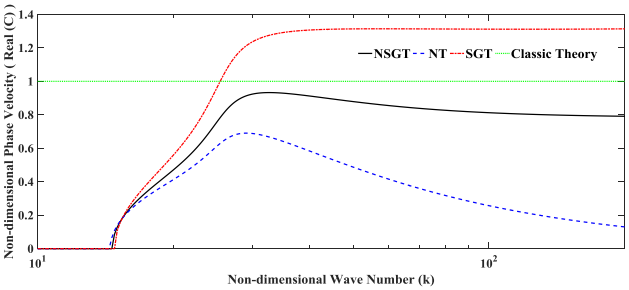

Fig. 2 Comparison of phase velocity of wave propagation in sandwich nano-beam obtained using different elasticity theories

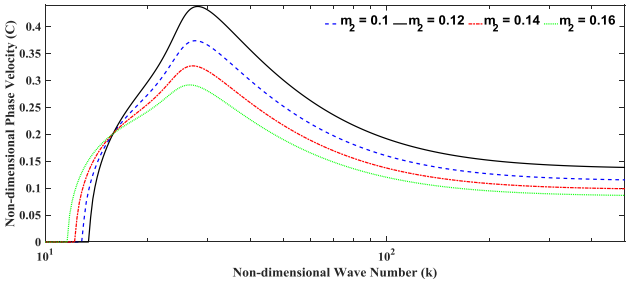

(a) real part

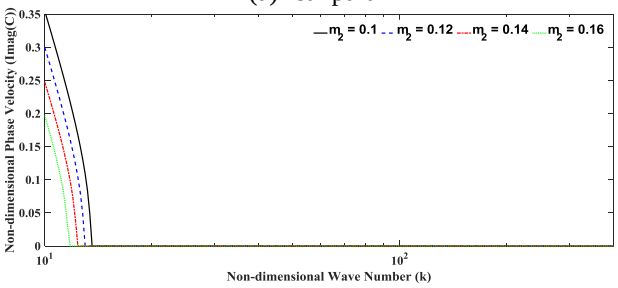

(b) imaginary part

Fig. 3 Non-dimensional Phase Velocity of the wave propagation in terms of various nonlocal parameters, $V_{CN}^* = 0.17$, $\eta = 0.142$, $\bar{H}_x = 1E+07$, $E_0 = 3.3E-03$.

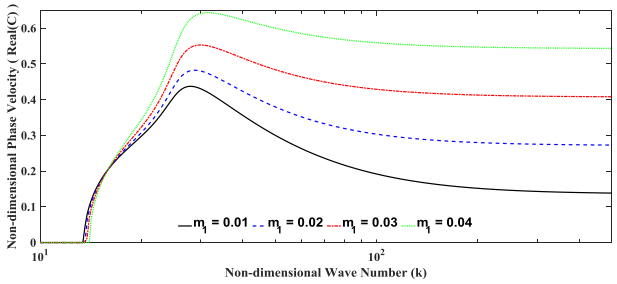

(a) real part

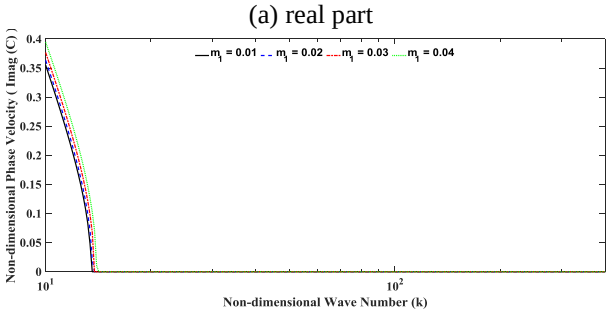

(b) imaginary part

Fig. 4 Non-dimensional Phase Velocity of the wave propagation in terms of various strain gradient parameters; a: real part b: imaginary part, $V_{CN}^* = 0.17$, $\eta = 0.142$, $\bar{H}_x = 1E+07$, $E_0 = 3.3E-03$

The influences of non-dimensional strain gradient parameter on phase velocity are investigated in Fig. 4. Regarding to results, the phase velocity of wave propagation decreases with increasing strain gradient parameter in small wave numbers range.

Table 2 The comparison between obtained results in present work and results yielded from exact solution and MTS method in Ref.(Gheshlaghi and Hasheminejad 2011, Nayfeh and Mook 2008)

μ_2	DQM	Exact solution	error	DQM	MTS Method	error
0.2	9.88	9.88	0.02%	9.88	9.88	0.001%
0.18	9.89	9.9	0.08%	9.9	9.89	0.004%
0.16	9.93	9.95	0.19%	9.93	9.93	0.007%
0.14	9.98	10.01	0.33%	9.98	9.98	0.010%
0.12	10.04	10.09	0.51%	10.04	10.04	0.010%
0.1	10.11	10.18	0.72%	10.11	10.11	0.004%
0.08	10.19	10.29	0.97%	10.19	10.20	-0.012%
0.06	10.29	10.42	1.24%	10.29	10.30	-0.040%
0.04	10.40	10.56	1.54%	10.40	10.41	-0.085%
0.02	10.52	10.72	1.86%	10.52	10.54	-0.149%

Unlike to above condition, increasing strain gradient parameter causes that phase velocity enhances in large wave numbers range. Also, phase velocity is equal to zero until wave number about 15 hereafter it started to increase up to wave number about 28 then begins decreasing. Fig. 5 represents non-dimensional phase velocity of wave propagation in sandwich nano-beam for different symmetric CNTs distributions in top and bottom face-sheets. According to this figure, phase velocity of wave propagation relative to UU pattern is larger than Phase velocity of wave propagation corresponding to VA and AV patterns in large wave numbers range, respectively. Whilst, phase velocity corresponding to VA pattern is greater than other patterns in wave numbers range about 15 to 22. This is a main point; AV pattern has less phase velocity in the whole range of wave number. The effects of the CNTs volume fraction on the phase velocity are investigated in Fig. 6 for two UU and AV patterns. In both aforementioned patterns, increasing the volume fraction causes that phase velocity of wave propagation in the sandwich nano-beam enhances. Therefore, this result indicates CNTs have important effects to control wave propagation in sandwich nano-beam.

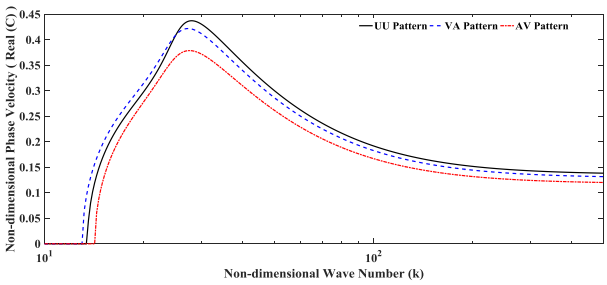

Fig. 5 Non-dimensional Phase Velocity of wave propagation in sandwich nano-beam for different symmetric CNTs Patterns; $\mu_1 = 0.01$, $\mu_2 = 0.1$, $V_{CN}^{*} = 0.17$, $\eta = 0.142$, $\bar{H}_x = 1E+07$, $E_0 = 3.3E-03$

Fig. 7 indicates non-dimensional phase velocity of wave propagation in sandwich nano-beam for different asymmetric CNTs patterns in top and bottom face-sheets with respect to natural geometric axis. Regarding to the obtained results, UA and UV patterns approximately have same phase velocity in whole range of wave number. As can be seen, phase velocity has a sudden and large increase in non-dimensional wave number equal to about 25 and phase velocity has a decreasing continuous curve in the other wave number values. In entire wave numbers range except in the range of 15 to 25, Phase velocity is equal to zero.

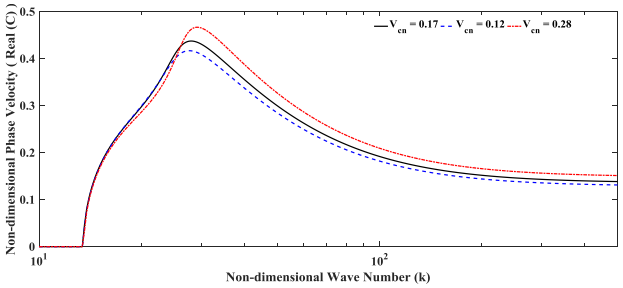

(a) UU Pattern

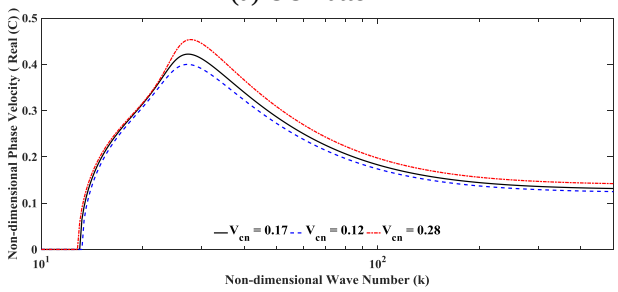

(b) AV Pattern

Fig. 6 Non-dimensional Phase Velocity of wave propagation in sandwich nano-beam for different volume fractions of CNTs; $\mu_1 = 0.01$, $\mu_2 = 0.1$, $\bar{H}_x = 1E+07$, $E_0 = 3.3E-03$

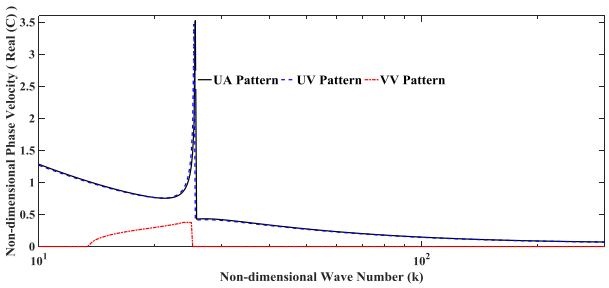

Fig. 7 Non-dimensional Phase Velocity of wave propagation in sandwich nano-beam for different asymmetric CNTs Patterns; $\mu_1 = 0.01$, $\mu_2 = 0.1$, $V_{CN}^{*} = 0.17$, $\eta = 0.142$, $\bar{H}_x = 1E+07$, $E_0 = 3.3E-03$

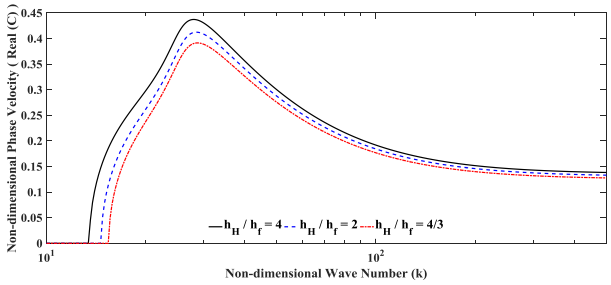

Fig. 8 Non-dimensional Phase Velocity versus Non-dimensional Wave Number for various non-symmetric CNTs Pattern; $\mu_1 = 0.01$, $\mu_2 = 0.1$, $V_{CN}^{*} = 0.17$, $\eta = 0.142$, $\bar{H}_x = 1E+07$, $E_0 = 3.3E-03$

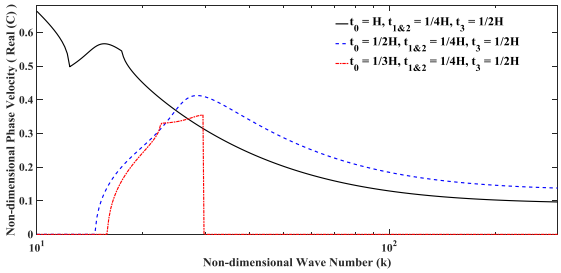

Fig. 9 Non-dimensional Phase Velocity of wave propagation in sandwich nano-beam for different asymmetric thicknesses of the face-sheets corresponding to UU pattern; $\mu_1 = 0.01$, $\mu_2 = 0.1$, $V_{CN}^{*} = 0.17$, $\eta = 0.142$, $\bar{H}_x = 1E+07$, $E_0 = 3.3E-03$

The influences of face-sheets to core thickness ratio on phase velocity are investigated in Fig. 8. According to presented results, decreasing ratio of face-sheet thickness to core thickness leads to decrease phase velocity of wave propagation in all of the wave numbers.

According to results presented in Fig. 9 it can be concluded that the thickness of the face-sheets have significant effects on phase velocity. As the thickness of the face-sheets (in this figure bottom face-sheet) is becoming smaller, the phase velocity becomes less and for some values of wave number becomes zero.

Phase velocity of wave propagation in the sandwich nano-beam is plotted versus corresponding wave numbers in Fig. 10 for different HSDBTs. According to these results, it can be deduced that phase velocity of wave propagation has approximately same values for all of the HOSDBTs in large wave numbers range whilst the difference between values of the phase velocity calculated for different HSDBTs is significant in small wave number range. Also among various HSDBTs, ESDBT and ASDBT exactly have the same values in whole wave number range and possess large phase velocity in lower value of the wave number with respect to other theories.

Phase velocity versus wave frequency is presented in Fig. 11 for different FG-CNTs patterns. As can be seen in this figure, the phase velocity leads to zero at a certain frequency when the wave number leads to large value. Its value can be called cut-off frequency (Ghorbanpour Arani Kolahchi *et al.* 2014). UU and VA patterns have the same cut-off frequency but AV pattern has the lower value with respect to them.

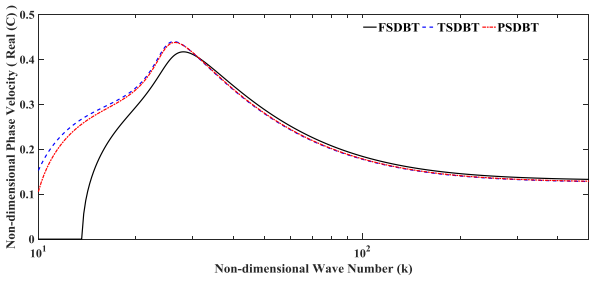

(a) FSDBT, TSDBT and PSDBT

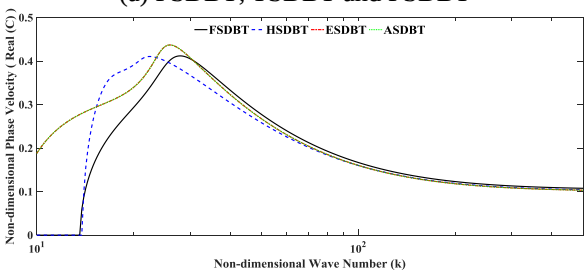

(b) FSDBT, HSDBT, ESDBT and ASDBT

Fig. 10 Non-dimensional Phase Velocity of wave propagation in sandwich nano-beam for different beam theories; $\mu_1 = 0.01$, $\mu_2 = 0.1$, $V_{CN}^{*} = 0.17$, $\eta = 0.142$, $\bar{H}_x = 1E+07$, $E_0 = 3.3E-03$

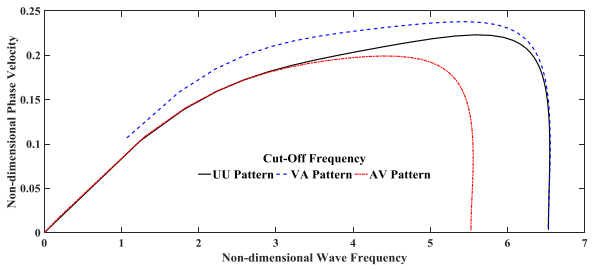

Fig. 11 Non-dimensional Phase Velocity of wave propagation versus Non-dimensional Wave Frequency for different CNTs patterns; $\mu_1 = 0.01$, $\mu_2 = 0.1$, $V_{CN}^{*} = 0.17$, $\eta = 0.142$, $\bar{H}_x = 1E+07$, $E_0 = 3.3E-03$

Fig. 12 illustrated phase velocity versus wave number in order to investigate effect of the Winkler and Pasternak coefficients. They have same effects on the phase velocity of wave propagation in sandwich nano-beam. According to the results, increasing aforementioned parameters causes the phase velocity increases in small wave numbers range whilst they have no effects in large wave numbers range.

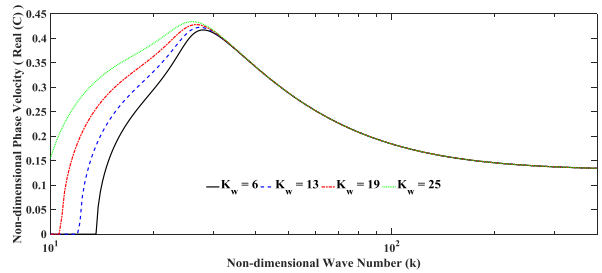

(a) Winkler Coefficient K_w

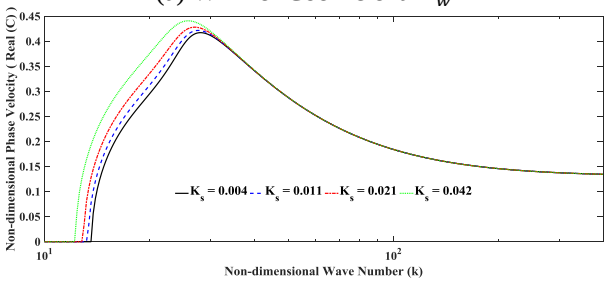

(b) Shearing Coefficient K_s

Fig. 12 Non-dimensional Phase Velocity of wave propagation in sandwich nano-beam for different Winkler and Pasternak coefficients

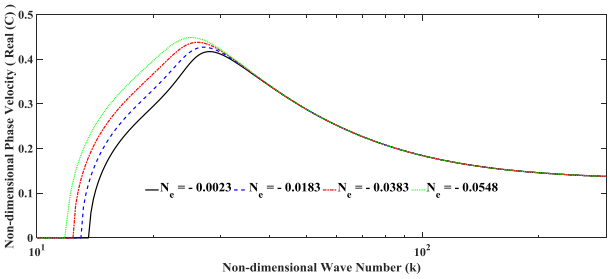

(a) Real part of the phase velocity for different Thermal Loads (N_t)

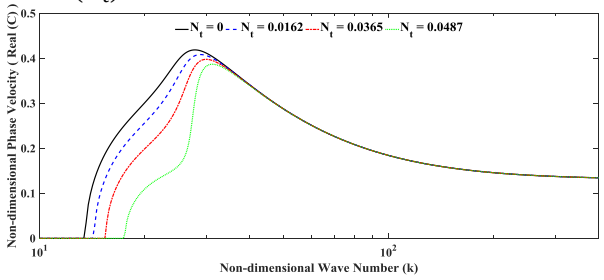

(b) Real part of the phase velocity for different Electrical Loads (N_e)

Fig. 13 Non-dimensional Phase Velocity of the wave propagation in sandwich nano-beam

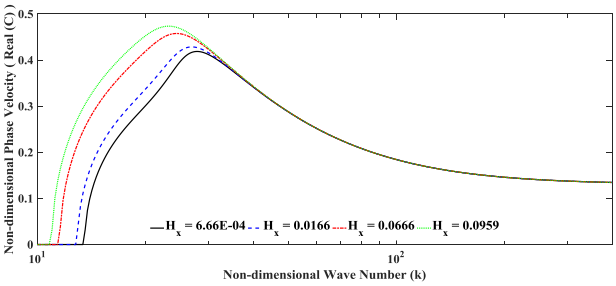

Fig. 14 Non-dimensional Phase Velocity of the wave propagation versus Non-dimensional Wave Frequency for different Magnetic loads H_x

The effects of the axial force established by temperature change and constant applied voltage on phase velocity are studied in Fig. 13. It is can be concluded that the applied voltage and rise temperature have the different influences on phase velocity. Regarding to results, increasing the applied voltage leads to enhance the phase velocity. It is worthy noted that aforementioned effect enhances in lower wave numbers range.

Regarding to results obtained in Fig. 14, the Enhancing magnetic field causes phase velocity of wave propagation increases in small wave numbers range.

7. Conclusions

Analysis of the wave propagation of the sandwich nano-beams with FG-CNTs face-sheets was implemented in this investigation. For first time, the different HSDBTs were employed to investigate propagation wave of the sandwich nano-beams with FG-CNTs face-sheets. Also the applied voltage, temperature rising, magnetic field, pretension and the nonlocal strain gradient theory to involve the nonlocal and strain gradient parameters was considered in deriving the equations of motion. Then, the governing equations were solved by the analytical method and the non-dimensional phase velocity for wave propagation was obtained. The effects of some parameters such as length scale parameters, different distribution pattern of CNTs in face-sheets, parameters of elastic-Pasternak foundation, applied voltage, different HSDBTs and other important parameters in designing and controlling the phase velocity were studied in detail. The most important results of this study are presented as:

1. Patterns of the CNTs in face-sheets have significant effects on cut-off frequency as UU and VA patterns possess the same cut-off frequency value but AV pattern has the lower value with respect to them.
2. Volume fraction of the CNTs in face-sheets can strongly change the non-dimensional phase velocity in sandwich nano-beam. The results indicate that phase velocity for different HSDBTs is increased with increasing the volume fraction of CNTs. Also it is deduced that the phase velocity of wave propagation relative to UU pattern is larger than phase velocity corresponding to AV and VA patterns.

3. The small scale parameters have significant effects on the phase velocity of the sandwich nano-beam with FG-CNTRC face sheets. It is observed that increasing nonlocal parameter causes phase velocity increases in very small wave numbers range whilst phase velocity decreases in larger wave numbers range. In addition, Increasing strain gradient parameter leads to enhance phase velocity in a large wave numbers range whilst increasing strain gradient causes phase velocity decreases in small wave numbers range.
4. Investigation on the effect of the elastic-Pasternak foundation parameters on the wave propagation of the sandwich nano-beam leads to important conclusions. Increasing the Winkler (K_w) and shearing (K_s) coefficients caused that the phase velocity increases in lower wave number and also they have no effects in larger wave number range.
5. According to obtained results, the constant applied voltage, longitudinal magnetic field and increment temperature have important influences on phase velocity. Enhancing the longitudinal magnetic field intensity and applied voltage leads to increase phase velocity of wave propagation. In addition, temperature rising causes phase velocity decreases in small wave numbers range.
6. According to results, the phase velocity of wave propagation calculated for different HSDBTs approximately has the same values in large wave numbers range. In small wave numbers range, difference between phase velocities for various high order theories is significant. Also among various HSDBTs, ESDBT and ASDBT exactly have the same values in whole wave number range and possess large phase velocity in lower value of the wave number with respect to other theories.

8. Abbreviation

FG	functionally graded
CNTs	carbon nanotubes
MTS	Multiple Times Scale
UD	uniform distribution
SWCNT	single-walled carbon nanotube
CNTRCs	carbon nanotube-reinforced composites

Acknowledgments

The author would like to thank the reviewers for their comments and suggestions to improve the clarity of this article. This work was supported by University of Kashan [Grant Number 574600/30].

References

Ansari, R., Shojaei, M.F., Mohammadi, V., Gholami, R. and Darabi, M.A. (2014), "Nonlinear vibrations of functionally graded mindlin microplates based on the modified couple stress theory", *Compos Struct.*, **114**, 124–134.

Ansaria, R., Mohammadia, V., Faghih Shojaeia, M., Gholamib, R. and Sahmania, S. (2014), "On the forced vibration analysis of Timoshenko nanobeams based on the surface stress elasticity theory", *Compos. Part B: Eng.*, **60**, 158-166.

Arefi, M. and Zenkour, A.M. (2017), "Thermo-electro-mechanical bending behavior of sandwich nanoplate integrated with piezoelectric face-sheets based on trigonometric plate theory", *Compos. Struct.*, **162**, 108-122.

Arefi, M. and Zenkour, A.M. (2017), "Vibration and bending analysis of a sandwich microbeam with two integrated piezo-magnetic face-sheets", *Compos. Struct.*, **159**, 479-490.

Arvin, H. and Bakhtiari-Nejad, F. (2013), "Nonlinear free vibration analysis of rotating composite Timoshenko beams", *Compos. Struct.*, **96,** 29-43.

Ashrafi, B. and Hubert, P. (2006), "Vengallatore S. Carbon nanotube-reinforced composites as structural materials for microactuators in microelectromechanical systems", *Nanotechnology*, **17**, 4895-4903.

Chen, H., Li, X.P., Chen, Y.Y. and Huang, G.L. (2017), "Wave propagation and absorption of sandwich beams containing interior dissipative multi-resonators", *Ultrasonics*, **76**, 99-108.

Ding, L., Zhu, H.P. and Wu, L. (2016), "Effects of axial load and structural damping on wave propagation in periodic Timoshenko beams on elastic foundations under moving loads", *Phys. Lett. A*, **380**(32), 2335-2341.

Ebrahimy. F. and Hosseini, S.H. (2016), "Nonlinear electroelastic vibration analysis of NEMS consisting of double-viscoelastic nanoplates", *Appl. Phys. A*, in press. doi: 10.1007/s00339-016-0452-6

Eltahera, M.A., Khaterb, M.E. and Emam, S.A. (2016), "A review on nonlocal elastic models for bending, buckling, vibrations, and wave propagation of nanoscale beams", *Appl. Math. Model.*, **40**(6), 4109-4128.

Esawi, A. and Farag, M. (2007), "Carbon nanotube reinforced composites: potential and current challenges", *Mater. Des.*, **28**, 2394-2401.

Gheshlaghi, B. and Hasheminejad, S.M. (2011), "Surface effects on nonlinear free vibration of nanobeams", *Compos. Part B: Eng.*, **42**, 934-937.

Gholami, R., Darvizeh, A., Ansari, R. and Hosseinzadeh, M. (2014), "Sizedependent axial buckling analysis of functionally graded circular cylindrical microshells based on the modified strain gradient elasticity theory", *Meccanica*, **49**(7), 1679-1695.

Ghorbanpour Arani, A., Jalilvand, A. and Kolahchi, R. (2014), "Wave propagation of magnetic nanofluid-conveying double-walled carbon nanotubes in the presence of longitudinal magnetic field", *Proc IMechE Part N: J Nanoengineering and Nanosystems*, **228**(2), 82–92.

Ghorbanpour Arani, A., Jamali, M., Ghorbanpour Arani, A.H., Kolahchi, R. and Mosayyebi, M. (2016), "Electro-magneto wave propagation analysis of viscoelastic sandwich nanoplates considering surface effects", *Proc IMechE Part C: J Mechanical Engineering Science*, 1–17. In press, doi: 10.1177/0954406215627830.

Ghorbanpour Arani, A., Kolahchi, R. and Esmailpour, M. (2016), "Nonlinear vibration analysis of piezoelectric plates reinforced with carbon nanotubes using DQM", *Smart Struct. Syst.*, **18(**4), 787-800.

Ghorbanpour Arani, A., Jamali, M., Mosayyebi, M. and Kolahchi, R. (2015), "Analytical modeling of wave propagation in viscoelastic functionally graded carbon nanotubes reinforced piezoelectric microplate under electro-magnetic field", *Proc IMechE Part N: J Nanoengineering and Nanosystems*, 1–17. In press, doi: 10.1177/1740349915614046.

Ghorbanpour Arani, A., Kolahchi, R. and Mortazavi, S.A. (2014), "Nonlocal piezoelasticity based wave propagation of bonded double-piezoelectric nanobeam-systems", *Int. J. Mech. Mater.*

Des., **10**, 179-191.
Ghorbanpour Arani, A., Kolahchi, R., Mosallaie Barzoki, A.A., Mozdianfard, M.R. and Noudeh Farahani, M. (2012), "Elastic foundation effect on nonlinear thermo-vibration of embedded double-layered orthotropic graphene sheets using differential quadrature method", *Proc IMechE Part C: J Mechanical Engineering Science*, 1–18. in press. doi: 10.1177/0954406212453808
Ghorbanpour Arani, A., Vossough, H. and Kolahchi, R. (2015), "Nonlinear vibration and instability of a visco-Pasternak coupled double-DWBNNTs-reinforced microplate system conveying microflow", *J. Mech. Eng. Sci*., 1-17.
Ghorbanpour Arani, A., Vossough, H., Kolahchi, R. and Mosallaie Barzoki, A.A. (2012), "Electro-thermo nonlocal nonlinear vibration in an embedded polymeric piezoelectric micro plate reinforced by DWBNNTs using DQM", *J. Mech. Sci. Technol.*, **26**(10), 3047~3057.
Joglekar, D.M. and Mitra, M. (2016), "Analysis of flexural wave propagation through beams with a breathing crack using wavelet spectral finite element method", *Mech. Syst. Signal Pr.*, **77**, 576-591.
Kanani, A.S., Niknam, H., Ohadi, A.R. and Aghdam, M.M. (2014), "Effect of nonlinear elastic foundation on large amplitude free and forced vibration of functionally graded beam", *Compos. Struct.*, **115**, 60-68.
Ke, L-L., Yang, J. and Kitipornchai, S. (2010), "Nonlinear free vibration of functionally graded carbon nanotube-reinforced composite beams", *Compos. Struct.*, **92,** 676-683.
Komijani, M., Esfahani, S.E., Reddy, J.N., Liu, Y.P. and Eslami, M.R. (2014), "Nonlinear thermal stability and vibration of pre/post-buckled temperature-and microstructure-dependent functionally graded beams resting on elastic foundation", *Compos. Struct.*, **112**, 292-307.
Li, J., Wu, Z., Kong, X., Li, X. and Wu, W. (2014), "Comparison of various shear deformation theories for free vibration of laminated composite beams with general lay-ups", *Compos. Struct*., **108,** 767-778.
Li, L. and Hu, Y. (2016), "Wave propagation in fluid-conveying viscoelastic carbon nanotubes based on nonlocal strain gradient theory", *Comput. Mater. Sci.*, **112**, 282-288.
Li, L., Hu, Y. and Ling, L. (2015), "Flexural wave propagation in small-scaled functionally graded beams via a nonlocal strain gradient theory", *Compos. Struct*., **133**, 1079-1092.
Li, L., Hu, Y. and Ling, L. (2015), "Wave propagation in viscoelastic single-walled carbon nanotubes with surface effect under magnetic field based on nonlocal strain gradient theory", *Physica E*, **75**, 118-124.
Li, L., Hu, Y. and Ling, L. (2016), "Wave propagation in viscoelastic single-walled carbon nanotubes with surface effect under magnetic field based on nonlocal strain gradient theory", *Physica E: Low-dimensional Systems and Nanostructures*, **75**, 118-124.
Liew, K.M., Hu, Y.G. and He, X.Q. (2008), "Flexural wave propagation in single-walled carbon nanotubes", *J. Comput. Theor Nanosci*, **5**(4), 581-586.
Liew, K. M., Yang, J., and Kitipornchai, S. (2003), "Postbuckling of piezoelectric FGM plates subject to thermo-electro-mechanical loading", *Int. J. Solids Struct.*, **40**, 3869-3892.
Lim, C.W., Zhang, G. and Reddy, J.N. (2015), "A higher-order nonlocal elasticity and strain gradient theory and its applications in wave propagation", *J. Mech. Phys. Solids*, **78**, 298-313.
Lim, C.W., Zhanga, G. and Reddy, J.N. (2015), "A higher-order nonlocal elasticity and strain gradient theory and its applications in wave propagation", *J. Mech. Phys.Solids*, **78**, 298-313.
Ma, L.H., Ke, L.L., Wang, Y.Z. and Wang, Y.S. (2017), "Wave propagation in magneto-electro-elastic nanobeams via two nonlocal beam models", *Physica E: Low-dimensional Systems and Nanostructures*, **86**, 253-261.
Mohammadimehr, M., Rousta Navi, B. and Ghorbanpour Arani, A. (2015), "Free vibration of viscoelastic double-bonded polymeric nanocomposite plates reinforced by FG-SWCNTs using MSGT, sinusoidal shear deformation theory and meshless method", *Compos. Struct.*, **131**, 654-671.
Natarajan, S., Haboussi, M. and Manickam, G. (2014), "Application of higher-order structural theory to bending and free vibration analysis of sandwich plates with CNT reinforced composite", *Compos. Struct.*, **113** 197-207.
Nateghi, A. and Salamat-talab, M. (2013), "Thermal effect on size dependent behavior of functionally graded microbeams based on modified couple stress theory", *Compos. Struct.*, **96**, 97-110.
Nayfeh, A.H. and Mook, D.T. (2008), *Nonlinear Oscillations*: Wiley-VCH.
Rafiee, M., He, X.Q. and Liew, K.M. (2014), "Non-linear dynamic stability of piezoelectric functionally graded carbon nanotube-reinforced composite plates with initial geometric imperfection", *Int. J. Nonlinear Mech.*, **59,** 37-51.
Rafiee, M., Yang, J. and Kitipornchai, S. (2013), "Large amplitude vibration of carbon nanotube reinforced functionally graded composite beams with piezoelectric layers", *Compos. Struct.*, **96,** 716-725.
Rabani Bidgoli, M., Karimi, M.S. and Ghorbanpour Arani, A. (2015), "Viscous fluid induced vibration and instability of FG-CNT-reinforced cylindrical shells integrated with piezoelectric layers", *Steel Compos. Struct*., **19**(3), 713-733.
Rahmani, O. and Jandaghian, A.A. (2015), "Buckling analysis of functionally graded nanobeams based on a nonlocal third-order shear deformation theory", *Appl Phy A*, **119**(3), 1019–1032.
Reddy, J. N. (2007), "Nonlocal theories for bending, buckling and vibration of beams", *Int. J. Eng. Sci.*, **45**, 288-307.
Schoeftner, J., Buchberger, G. and Benjeddou, A. (2016), "Slender piezoelectric beams with resistive-inductive electrodes – modeling and axial wave propagation", *Smart Struct. Syst.*, **18** (2), 335-354.
Shafiei, N., Kazemi. M. and Ghadiri, M. (2016), "Nonlinear vibration behavior of a rotating nanobeam under thermal stress using Eringen's nonlocal elasticity and DQM", *Appl. Phys. A*, in press.
Shakeri, M., Akhlaghi, M. and Hoseini, S.M. (2006), "Vibration and radial wave propagation velocity in functionally graded thick hollow cylinder", *Compos. Struct*., **76**(1), 174-181.
Shen, H.S. and Zhang, C.L. (2012), "Non-linear analysis of functionally graded fiber reinforced composite laminated plates, Part I: Theory and solutions", *Int. J. Nonlinear Mech.*, **47**, 1045-1054.
Simsek, M. and Reddy, J.N. (2013a), "Bending and vibration of functionally graded microbeams using a new higher order beam theory and the modified couple stress theory", *Int. J. Eng. Sci.*, **64**, 37-53.
Simsek, M. and Reddy, J.N. (2013b), "A unified higher order beam theory for buckling of a functionally graded microbeam embedded in elastic medium using modified couple stress theory", *Compos. Struct.*, **101**, 47-58.
Yang, F., Chong, A., Lam, D. and Tong, P. (2002), "Couple stress based strain gradient theory for elasticity", *Int. J. Solids Struct.*, **39**(10), 2731-2743.
Yang, Y. and Lim, C.W. (2012), "Non-classical stiffness strengthening size effects for free vibration of a nonlocal nanostructure", *Int. J. Mech. Sci.*, **54**, 57-68.
Zhang, Z.J. and Paulino, G.H. (2007), "Wave propagation and dynamic analysis of smoothly graded heterogeneous continua using graded finite elements", *Int. J. Solids Struct.*, **44**(11), 3601–3626.

CC